Chemical Engineering & Technology

LES of bubble column bubbly flows accounting SGS turbulent dispersion and added mass stress effects

Journal:	*Chemical Engineering & Technology*
Manuscript ID	ceat.202300142.R1
Wiley - Manuscript type:	Research Article
Date Submitted by the Author:	n/a
Complete List of Authors:	Long, Shanshan; University of Nottingham Ningbo China, Mechanical, Materials and Manufacturing Engineering Yang, Xiaogang; Univ Nottingham Ningbo China, Mechanical, Materials and Manufacturing Engineering Yang, Jie; University of Hull, School of Natural Sciences Sommerfeld, Martin; Otto von Guericke Universitat Magdeburg, Fakultät für Verfahrens- und Systemtechnik Xue, Chenyang; University of Nottingham Ningbo China
Keywords:	Added Mass Stress, Bubble Column, LES Simulation, Mass transfer, Turbulent Dispersion

Shanshan Long[1]

Xiaogang Yang[1,*]

Jie Yang[2]

Martin Sommerfeld[3]

Chenyang Xue[1]

LES of bubble column bubbly flow considering SGS turbulent diffusion effect and bubble oscillation

The present study will demonstrate through Euler/Euler LES modelling that turbulent dispersion of bubbles can effectively indicate the impact of turbulent eddies on bubble dynamics, i.e. the bubble oscillation behavior. This finding builds on previous work using Euler/Lagrange LES modelling approach and leads to a significant improvement in predicting bubble lateral dispersion. Spatially filtered terms were proposed for the SGS turbulent dispersion and added mass stress force models, with a modification made to the SGS eddy viscosity to reflect bubble turbulent dispersion and oscillations. The proposed model substantially improves the prediction of bubble volume fraction distribution, bubble and liquid phase velocity profiles, turbulent kinetic energy spectrum, and mass transfer.

Keywords: Added Mass Stress, Bubble Column, LES Simulation, Mass Transfer, Turbulent Dispersion

[1]Department of Mechanical, Materials and Manufacturing Engineering, The University of Nottingham Ningbo China, University Park, Ningbo 315100, PR China
[2]School of Natural Sciences, University of Hull, Hull HU6 7RX, UK
[3]Faculty of Process and Systems Engineering, Otto-von-Guericke-Universität Magdeburg, Zeppelinstraße 1, 06130 Halle, Magdeburg, Germany

*Corresponding author: Professor Xiaogang Yang Email: Xiaogang.Yang@nottingham.edu.cn

1. Introduction

When applying two-fluid model Euler/Euler large eddy simulation, the filtering process involves the use of phasic 'function of presence' approach to the momentum equation by accounting for co-sharing of a control volume by different phases. As a result, this leads to the terms denoting interfacial momentum forces, contributed by the dot product of total stress term and gradient of 'function of presence' term, and indicates the forces induced by the local flow perturbations at the interface of the second phase (bubbles). The subsequent averaging (ensemble averaging for RANS turbulence or spatial filtering for LES model) to the momentum equation and the interfacial momentum terms leads to the additional terms that can be attributed to the drag and other parts that can be modelled as non-drag forces such as lift force, added mass force and turbulent dispersion force (SGS-TDF) together with the added mass stress force (SGS-AMS). In case of conducting two-phase LES, these interfacial momentum exchange terms need to be modelled in terms of the resolved quantities of the flow or filtered variables while taking into account the effect of unresolved fluctuating on sub-grid scale. It should be mentioned that most of the previously reported work on two-phase or three-phase LES has overlooked or neglected the unresolved sub-grid scale contributions. Several previous studies have also indicated the important role played by the turbulence terms of the interfacial momentum transfer on the bubble dynamics, in particular related to the added mass stress force which has proved to be effective in improving the phase distribution prediction, e.g. bubbly mixing layer [1], air-lift [2], and vertical liquid-liquid pipe flows [3].

Due to the bubble's dynamic response to the surrounding carrier phase, the bubble mass centre changes with its entrainment, which leads to bubble oscillations and tumbling motion [4]. To consider the bubble dynamic motion using Euler/Euler LES modelling approach, one may interpret that the interactions between bubble and the surrounding turbulent eddies give rise to the bubble deformation in case of no bubble coalescence or break-up taking place as shown in Figure 1. Thus, the interphase forces acting on the dispersed phase are strongly affected by interactions between the bubbles and the turbulent shear caused by nearby turbulent eddies, and these interfacial momentum transfer must be properly implemented in the sub-grid scale LES [5-9].

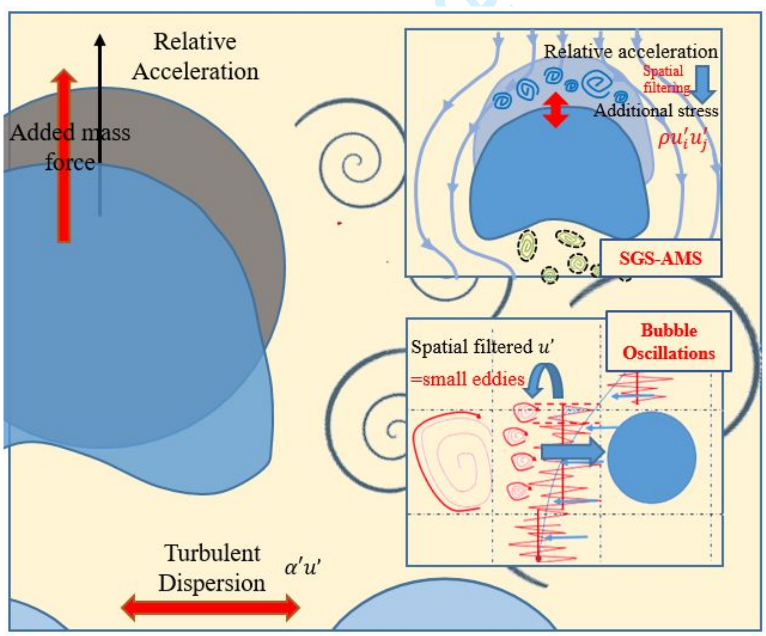

Figure 1

By taking both phase velocity fluctuations and bubble volume fraction fluctuations into account, the spatial filtering of the drag force and added mass force terms will give rise to the extra terms proportional to the area density and slip velocity correlation i.e., turbulent dispersion, and the correlation of bubble volume fraction and gradient of SGS stress. Based on the SGS eddy diffusivity hypothesis, the SGS-TDF and SGS-AMS will be used to mimic the turbulent dispersion effect in the framework of Euler/Euler two-fluid model approach, revealing the bubble dynamics in the bubble column in the present study. The modified SGS eddy viscosity ν_T accounting for the bubble dynamic response to the turbulent eddies induced shear will be implemented in modelling the SGS-TDF and SGS-AMS terms [10].

2. Mathematical modelling and numerical methods

2.1 Governing equations

The two-fluid model based LES modelling has been adopted in the present study. By applying the phase-weighted filtering to mass and momentum conservation equations, the governing equations can be written as

$$\frac{\partial}{\partial t}(\rho_k\alpha_k) + \nabla\cdot(\alpha_k\rho_k\boldsymbol{u}_k) = 0 \quad (1)$$

$$\frac{\partial}{\partial t}(\alpha_k\rho_k\boldsymbol{u}_k) + \nabla\cdot(\alpha_k\rho_k\boldsymbol{u}_k\boldsymbol{u}_k) = -\nabla\cdot(\alpha_k\boldsymbol{\tau}_k) - \alpha_k\nabla p + \alpha_k\rho_k g + \boldsymbol{M}_{F,k}\,. \quad (2)$$

where $\boldsymbol{u}_k$ is the filtered velocity vector for phase k in grid-scale, given as $\tilde{\boldsymbol{u}}_k = \boldsymbol{u}_k + u_k'$ while $\tilde{\boldsymbol{u}}_k$ is the instantaneous velocity and $\boldsymbol{u}_k'$ stands for the sub-grid scale (SGS) fluctuation, which needs to be modelled. The terms on the right-hand side of Equation (2) respectively represent the stress, the pressure gradient, gravity and the filtered interphase momentum exchange, which arises from the actions of the interphase forces. The stress term is given by

$$\tau_k = -\mu_{eff}\left(\nabla\boldsymbol{u}_k + (\nabla\mathbf{u}_\mathrm{k})^T - \frac{2}{3}I(\nabla\cdot\boldsymbol{u}_k)\right) \quad (3)$$

where μ_{eff} is the effective viscosity of the liquid phase, which may be assumed to be composed of the contributions from the molecular viscosity, the turbulent eddy viscosity and the bubble induced turbulence, i.e.

$$\mu_{eff} = \mu_{L,L} + \mu_{T,L} + \mu_{BI,L}\,. \quad (4)$$

The extra viscosity due to the bubble-induced turbulence is now usually modelled based on Sato's model, given by

$$\mu_{BI,L} = \rho_L C_{\mu,BI} \alpha_G d_B |\boldsymbol{u}_G - \boldsymbol{u}_L| \,. \tag{5}$$

However, as will be discussed later in this section, this viscosity due to the bubble-induced turbulence may also be contributed by the relative bubble dynamic response to those turbulent eddies that have equivalent or slightly larger length scale and entrapped the bubbles [11, 12]. The filtered momentum exchange term can be classified as different contributions from the interphase forces, defined by

$$\boldsymbol{M}_{F,L} = -\boldsymbol{M}_{F,G} = \boldsymbol{M}_{D,L} + M_{L,L} + \boldsymbol{M}_{AM,L} + \boldsymbol{M}_{TD,L} + \boldsymbol{M}_{AMS,L} \tag{6}$$

where the terms on the right-hand side of Equation (6) are interphase forces acting on the bubbles that are caused by the filtered drag, lift and added mass plus turbulence dispersion and so-called added mass stress. The formulations of the filtered drag, lift and added mass forces employed in the Euler/Euler LES modelling are summarised in Table 1.

Table 1

Forces	Expressions
Drag	$\boldsymbol{M}_{D,L} = \frac{3}{4}\alpha_G \rho_L \frac{C_D}{d_B}\lvert\boldsymbol{u}_G - \boldsymbol{u}_L\rvert(\boldsymbol{u}_G - \boldsymbol{u}_L)$, $C_D = \frac{2}{3}E_O^{\frac{1}{2}}$, $E_0 = \frac{g\Delta\rho d_B^2}{\sigma}$
Lift	$\boldsymbol{M}_{L,L} = \rho_L C_L(\boldsymbol{u}_B - \boldsymbol{u}_L)\times(\nabla\times\boldsymbol{u}_L)$, $C_L = \begin{cases} min[0.288tanh(0.121Re_B), f(E'_O)] & E'_O \leq 4 \\ f(E'_O) & 4 < E'_O < 10 \\ -0.29 & E'_O > 10 \end{cases}$ $E'_O = \frac{g(\rho_l - \rho_g)d_h^2}{\sigma}$, $d_h = d\left(1 + 0.163E_O'^{0.757}\right)^{1/3}$
Added mass	$\boldsymbol{M}_{AM,L} = \alpha_G \rho_L C_{AM}\left(\frac{D\boldsymbol{u}_G}{Dt} - \frac{D\boldsymbol{u}_L}{Dt}\right)$

The turbulent dispersion term $\boldsymbol{M}_{TD,L}$ can be obtained by phase-weighted filtering the instantaneous interphase drag force term, expressed by Equation (7) after taking a certain derivations and simplifications, given by

$$\boldsymbol{M}_{TD,L}=\frac{3}{4}\rho_G\frac{C_D}{d_G}|\boldsymbol{u}_G-\boldsymbol{u}_L|\left(\frac{\overline{\alpha_G'u_G'}}{\alpha_G}-\frac{\overline{\alpha_L'u_L'}}{\alpha_L}\right)=\frac{3}{4}\rho_G\frac{C_D}{d_G}|\boldsymbol{u}_G-\boldsymbol{u}_L|\frac{\nu_{SGS}}{\sigma_{SGS}}\left(\frac{\nabla\alpha_G}{\alpha_G}-\frac{\nabla\alpha_L}{\alpha_L}\right). \quad (7)$$

The bubble oscillation in the bubble column bubbly flow can be thought of as a result of the interactions between bubbles and the surrounding turbulent eddies in the frame of Eulerian-Eulerian modelling, leading to the deformation of the bubble shapes if bubbles are not subjected to coalescence and break-up. The liquid-phase turbulence eddy viscosity can be modified as the sum of the filtered turbulent shear and SGS eddy viscosities to reflect the modification due to bubble dynamic response to the turbulent eddies, i.e.

$$\mu_{T,L}=\rho_L(C_s\Delta)^2|S|\left(1+\mathrm{C_b}\alpha_G\frac{\lambda}{d_B}\left(\frac{1}{1+St_{SGS}}\right)^{\frac{3}{2}}\right) \quad (8)$$

where λ represents the different turbulent length scales in the range between the integral and Kolmogorov scales ($L>\lambda>\eta$), *Cs* is a model constant, *S* is the characteristic filtered rate of strain tensor and St_{SGS} is the local Stokes number expressed as $St_{SGS}=\frac{\tau_{\mathrm{bubble}}}{\tau_{L,SGS}}$. The bubble response time scale can be estimated using $\tau_{\mathrm{bubble}}=\frac{4(\rho_G+0.5\rho_L)d_B^2}{3\mu_L C_D Re_B}$ while the characteristic time of turbulent eddies in sub-grid scale can be estimated by $\tau_{L,SGS}=\frac{\Delta}{\boldsymbol{u}'_{\mathrm{L,SGS}}}$. Since $\alpha_L+\alpha_G=1$ in two-phase flow system and $\nabla\alpha_L+\nabla\alpha_G=0$, this would yield Equation (9):

$$\boldsymbol{M}_{TD,L}=C_{TD}\frac{3}{4}\rho_G\alpha_G\frac{C_D}{d_G}|\boldsymbol{u}_G-\boldsymbol{u}_L|\frac{(C_s\Delta)^2|S|\left(1+C_b\alpha_G\frac{\Delta}{d_B}\left(\frac{1}{1+St_{SGS}}\right)^{\frac{3}{2}}\right)}{\sigma_A}\left(\frac{1}{\alpha_L}+\frac{1}{\alpha_G}\right)\nabla\alpha_L \quad (9)$$

For simplicity, Equation (9) is referred to as the modified sub-grid turbulent dispersion force model (SGS-TDF) hereafter. As shown in Figure 1, the filtering of the instantaneous added mass force will also result in the mean and turbulent contributions in SGS scale when taking the filtering to the instantaneous added mass force, which can be expressed as:

$$\overline{\chi_G\tilde{\boldsymbol{M}}_{AM,L}}=\overline{\chi_G\rho_L C_{AM}\left(\frac{D\boldsymbol{u}_L}{Dt}-\frac{D\boldsymbol{u}_G}{Dt}\right)}=\alpha_G\rho_L C_{AM}\left(\frac{\partial\bar{\bar{\boldsymbol{u}}}_L}{\partial t}+\bar{\bar{\boldsymbol{u}}}_L\cdot\nabla\bar{\bar{\boldsymbol{u}}}_L-\frac{\partial\bar{\bar{\boldsymbol{u}}}_G}{\partial t}+\bar{\bar{\boldsymbol{u}}}_G\cdot\nabla\bar{\bar{\boldsymbol{u}}}_G\right)+\rho_L C_{AM}$$
$$\left(\nabla\cdot\alpha_G\overline{\overline{\boldsymbol{u}'_{L,i}\boldsymbol{u}'_{L,j}}}-\nabla\cdot\alpha_G\overline{\overline{\boldsymbol{u}'_{G,i}\boldsymbol{u}'_{G,j}}}\right)+\alpha_G\rho_L C_{AM}\left(\frac{\partial\overline{\overline{\boldsymbol{u}'_L}}}{\partial t}+\bar{\bar{\boldsymbol{u}}}_L\cdot\nabla\overline{\overline{\boldsymbol{u}'_L}}+\overline{\overline{\boldsymbol{u}'_L}}\cdot\nabla\bar{\bar{\boldsymbol{u}}}_L\right) \quad (10)$$

It should be noted that the consequence of applying spatial filtering to the added mass force would deal with the correlations such as $\overline{\overline{\alpha_k \boldsymbol{u}'_{k,i}\boldsymbol{u}'_{k,j}}}$ as indicated in the second and third parts of the right-side of Equation (10), which functions like the Reynolds stress but also correlates with the local bubble volume fractions. It is referred to as the SGS added mass stress (SGS-AMS). By employing the eddy diffusivity hypothesis, the SGS added mass stress (SGS-AMS) can be written as

$$\mathbf{M}_{\mathrm{AMS}} = \alpha_{\mathrm{G}}\rho_{\mathrm{L}}\mathrm{C}_{\mathrm{AM}}\left(\frac{\nabla\cdot(\alpha_{\mathrm{L}}\boldsymbol{\tau}_{\mathbf{L}})}{\alpha_{\mathrm{L}}\rho_{\mathrm{L}}} - \frac{\nabla\cdot(\alpha_{\mathrm{G}}\boldsymbol{\tau}_{\mathrm{G}})}{\alpha_{\mathrm{G}}\rho_{\mathrm{G}}}\right)$$

$$= \alpha_{\mathrm{G}}\rho_{\mathrm{L}}\mathrm{C}_{\mathrm{AM}}\left[\frac{1}{\alpha_{\mathrm{L}}\rho_{\mathrm{L}}}\nabla\cdot\left(\alpha_{\mathrm{L}}\rho_L(1-\alpha_G)(C_S\Delta)^2|S_L|S_L\left(1+C_b\alpha_G\frac{\lambda}{d_B}\left(\frac{1}{1+St_{SGS}}\right)^{\frac{3}{2}}\right)\right) - \frac{1}{\alpha_{\mathrm{G}}\rho_{\mathrm{G}}}\nabla\cdot\left(\alpha_{\mathrm{G}}\rho_L(1-\alpha_G)(C_S\Delta)^2|\right.\right. \quad (18)$$

It would be expected that the SGS-AMS force will also have a significant impact on the bubble dynamics and interfacial mass transfer between the bubbles and liquid phase.

2.2 Experimental and numerical modelling

The proposed SGS turbulent dispersion and added mass stress models were tested by comparing the simulation results with the detailed experimental data as reported by Sommerfeld *et al.* [4] and the author's repeated experiment using the PIV. Both the modelled circular bubble column and the actual bubble column used in the experiments have an internal diameter of 140 mm, which was filled with a liquid level height of 0.65m. The experimental bubble column has a gas sparger that contains 50 evenly distributed capillaries at 0.4 mm in diameter, injecting the gas from the annular region within 100 mm in diameter. The gas flow rate was controlled by maintaining 160 L/H, corresponding to the averaged bubble volume fraction of 1.26% with the number-averaged bubble diameter of 2.55 mm. Both PIV (Dantec Dynamics) and a high-speed camera (Nikon AF-S 24mm f/1.8G ED) were used to obtain the bubble velocity and volume fraction distribution, as shown in Figure 2.

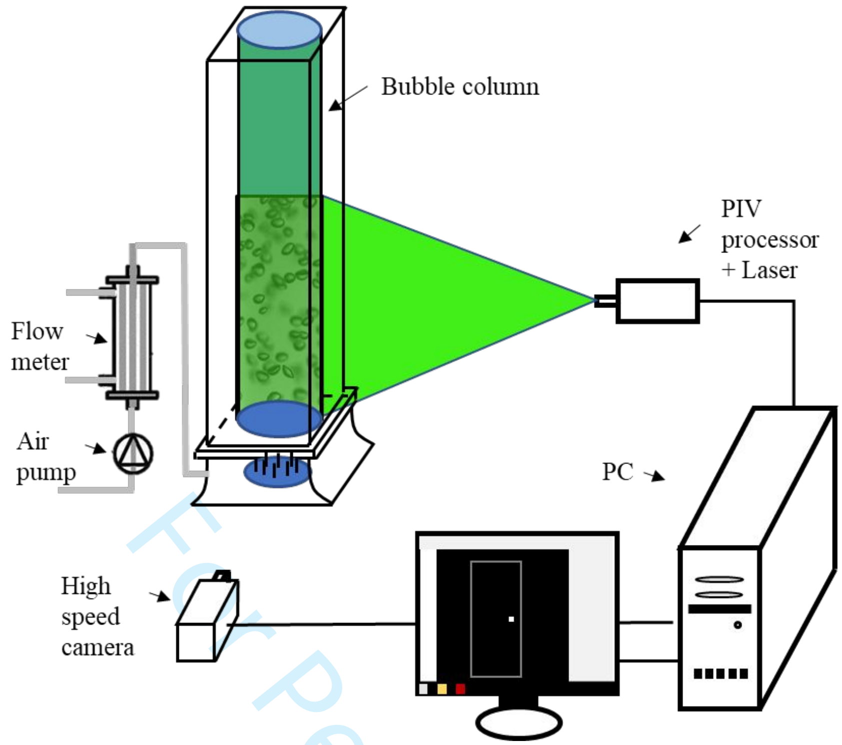

Figure 2

In the simulation, the number weighted bubble size distribution (BSD) among the entire bulk phase obtained in the experiment was adopted to account for the actual bubble size change. Considering bubble volume fraction for the present study $\alpha_G < 0.04$, the bubble number density transport may be more appropriately used to describe the bubble size distribution if bubbles move with small collision, negligible breakup and coalescence rates, given by

$$\frac{\partial n}{\partial t} + \nabla \cdot (\boldsymbol{u}_G \mathrm{n}) = 0. \tag{11}$$

The Sauter mean diameter can then be obtained by

$$d_{G,32} = \left(\frac{6\alpha_G}{\pi n}\right)^{1/3}. \tag{12}$$

As the local bubble equivalent diameter is in the same order as the SGS grid scales, therefore, the bubble size can be characterised with the 0-th moment of the bubble size distribution i.e., only taking the local mean bubble diameter, i.e. specification of one equivalent bubble diameter rather than a range of bubble sizes. This MUSIG approach requires much less computational effort and offers a surprisingly good agreement with available experimental data [13]. For Euler/Euler LES modelling, the boundary conditions were specified as described below. At inlet, a mass flow rate was specified, corresponding to the experimental conditions used by Sommerfeld *et al.* [4] and the author's experiment. At the top surface of the reactor, a pressure-constant boundary is specified. No-slip condition was applied to the inner wall of the bubble column. A central-differencing discretisation scheme was used for convective and diffusive terms in the momentum equations, while a second-order backward Euler scheme is employed for the transient term. The mesh set-up for the bubble column for the current LES modelling as shown in Figure 3 was satisfied the condition that the cell size of Δz^+=100 in the main flow direction and Δr^+=5 in the radial direction with a growth rate of 1.2 and total 95,400 cells. With caution and from the perspective of the computational cost, $\overline{d}_B/\Delta = 0.6375$ in the core-region was used in the LES modelling. This grid resolution adopted is considered to be reasonably close to Milelli's limit [14]. In the LES simulation, the time step δt_E was chosen in terms of CFL criterion, min($\frac{|\boldsymbol{u}_L|\delta t_E}{\Delta}$, $\frac{|\boldsymbol{u}_G-\boldsymbol{u}_L|\delta t_E}{\Delta}$)<1.0, varying from 0.0005 s to 0.001s for capturing the transient behaviour of turbulent eddy evolution in the bubble column. The simulations were run to last for 100 seconds while the instantaneous velocities at given positions were monitored and recorded during the calculation process.

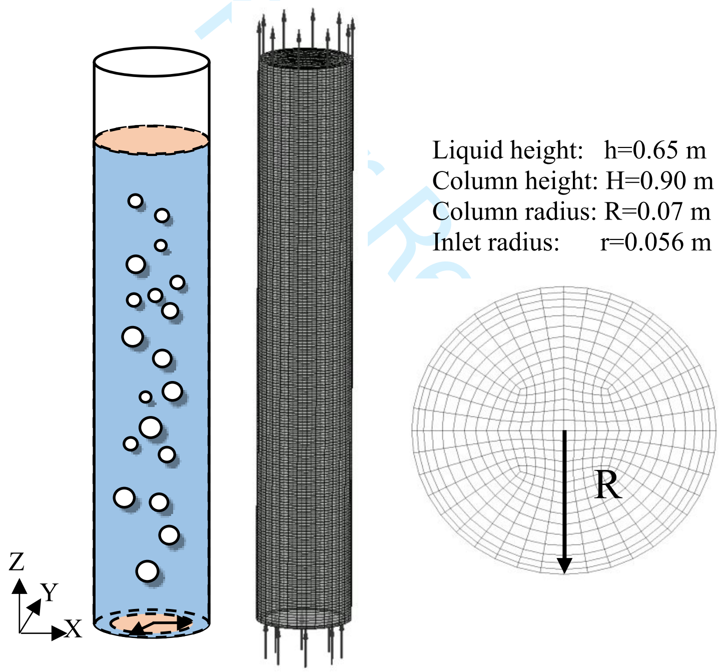

Figure 3

3. Results and discussion

3.1 Effects of accounting for the turbulent dispersion and added mass stress in LES on bubble transport

To highlight the importance of the turbulent dispersion and added mass stress in affecting the bubble transport in Eulerian-Eulerian LES modelling, the results obtained by using our modified SGS-TDF and SGS-

AMS models are also compared with those using Euler/Lagrange LES simulation [7] and experimental data as shown in Figure 4. The time-averaged bubble axial velocity profiles predicted by using the modified and standard turbulent dispersion force models at height *z*=0.325m are illustrated. Our Euler/Euler LES simulation has employed the forces that include the time averaged drag, lift, buoyancy, added mass forces together with the modified SGS-TDF and SGS-AMS (Cases 2: D+L+AM+SGS-TDF and Case 3: D+L+AM+SGS-TDF+SGS-AMS). It can be seen that the Euler/Euler LES by implementing either the modified SGS-TDF force or SGS-AMS models (Cases 2 and 3) performs better than the simple use of the momentum exchange terms, drag, lift and added mass forces (Cases 1), for prediction of the bubble velocity profiles.

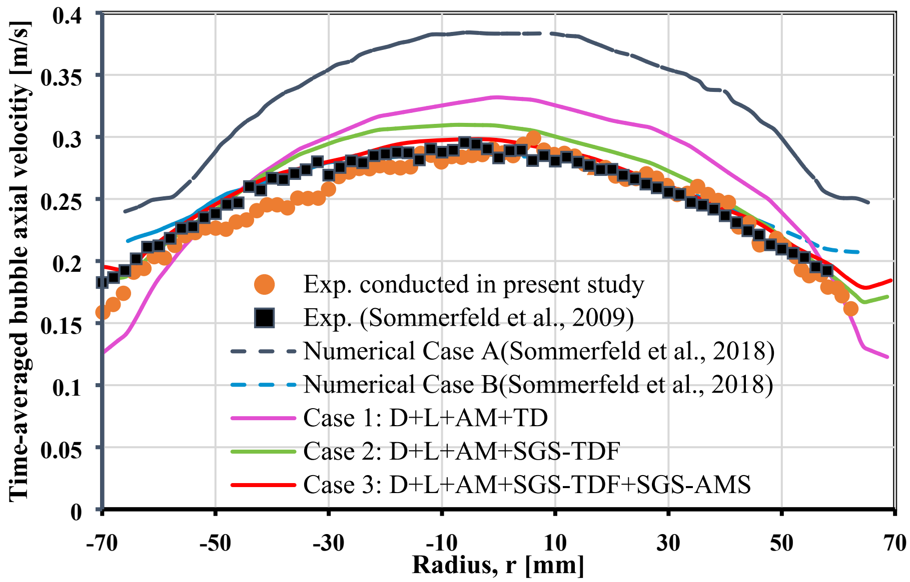

Figure 4

The bubble axial velocity profile predicted by neglecting the SGS-TDF and SGS-AMS contributions shows an apparent difference from the experimental result with over-prediction of the bubble axial velocity in the central core region but under-prediction of its value nearing the bubble column wall. This clearly demonstrates that the inclusion of the modified SGS-TDF and SGS-AMS in the LES simulation has a remarkable influence on the bubble radial dispersion. It can be observed from Figure 4 that the predicted profiles by using the modified SGS-TDF model and the modified SGS-TDF and SGS-AMS are consistent with their predicted velocity profiles, especially in the case that the SGS-AMS model is implemented into the modelling. The fact that the results obtained by considering the fluctuating $\overline{\alpha'_k \boldsymbol{u}'_k}$ and $\nabla \cdot \left(\alpha_k \overline{\overline{\boldsymbol{u}'_{k,i}\boldsymbol{u}'_{k,j}}}\right)$ with dynamic response to surrounding eddies are improved and are better consistent with the experimental results highlights the need for inclusion of the SGS-TDF and SGS-AMS for properly modelling bubble dispersion especially bubble radial migration in the bubble column bubbly flow. Figure 5 shows the time-averaged radial bubble volume fraction distribution obtained by using the standard SGS-TDF (Case 1), the modified SGS-TDF (Case 2) and the modified SGS-TDF plus SGS-AMS models (Case 3), compared with the Euler/Lagrange LES simulation results reported by Muniz and Sommerfeld [20]. This may be attributed to the inclusion of the modified SGS-TDF and SGS-AMS models that can effectively modulate the bubble lateral dispersion in the LES simulation.

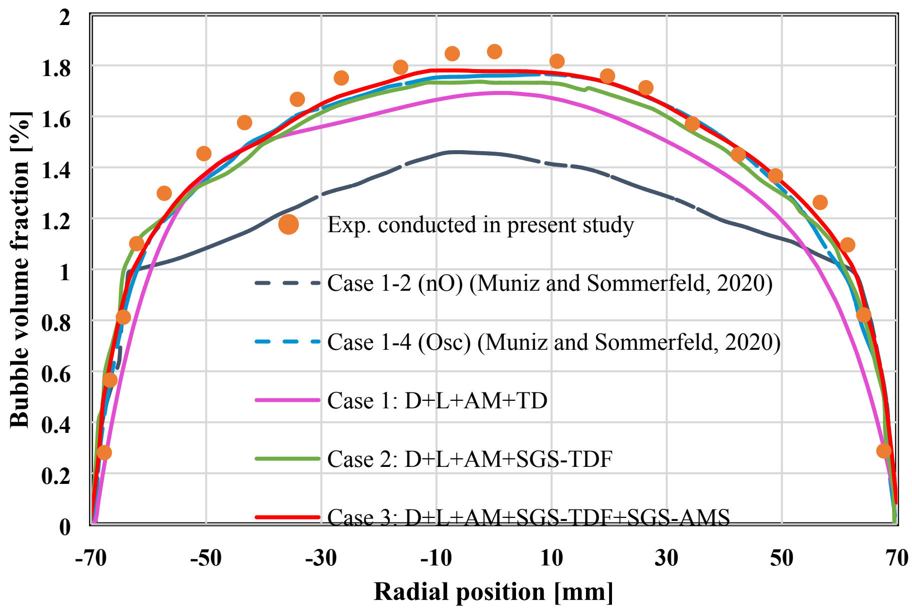

Figure 5

3.2 Quantification of SGS-turbulent dispersion force and added mass stress contributions and effect on bubble dynamics

To characterise the effect of the contributions from SGS-TDF and SGS-AMS on turbulent dispersion, the ratios of cross-sectional averaged SGS-TDF and added mass stress force to the overall sum of drag, lift and added mass forces at different cross-sections along the height of the bubble column have been obtained. Figure 6(a) shows the quantification of the ratio of the cross-sectional averaged SGS-TDF to the sum of drag, lift and added mass forces along the bubble column height. By comparing the magnitude of the contribution from drag, lift and added mass forces, along the height, the ratio can reach around 12% but gradually decreases with the height. The decrease in the ratio of the SGS-turbulent dispersion force to the overall contribution from drag, lift and added mass forces along the column height reveals that the bubble lateral dispersion is highly affected by the turbulent dispersion force, implying that a stronger SGS-TDF may promote the bubble group oscillations [4]. In terms of the ratio of total added mass stress force to the sum of the averaged drag, lift and added mass forces, the magnitude of the ratio can also reach 9% in the lower part of the bubble column but follows the same trend as the ratio of SGS-TDF to the sum of drag, lift and added mass forces as shown in Figure 6(b). Figure 7 shows the distribution of SGS-AMS and SGS-TDF terms obtained from the LES at different height in the bubble column together with the bubble volume fraction gradient and shear strain rate distribution from H=0.1-0.6m at t=100s. Thus, the present study has highlighted the importance of the contributions of SGS-TDF and SGS-AMS in the LES modelling of bubble column bubbly flow.

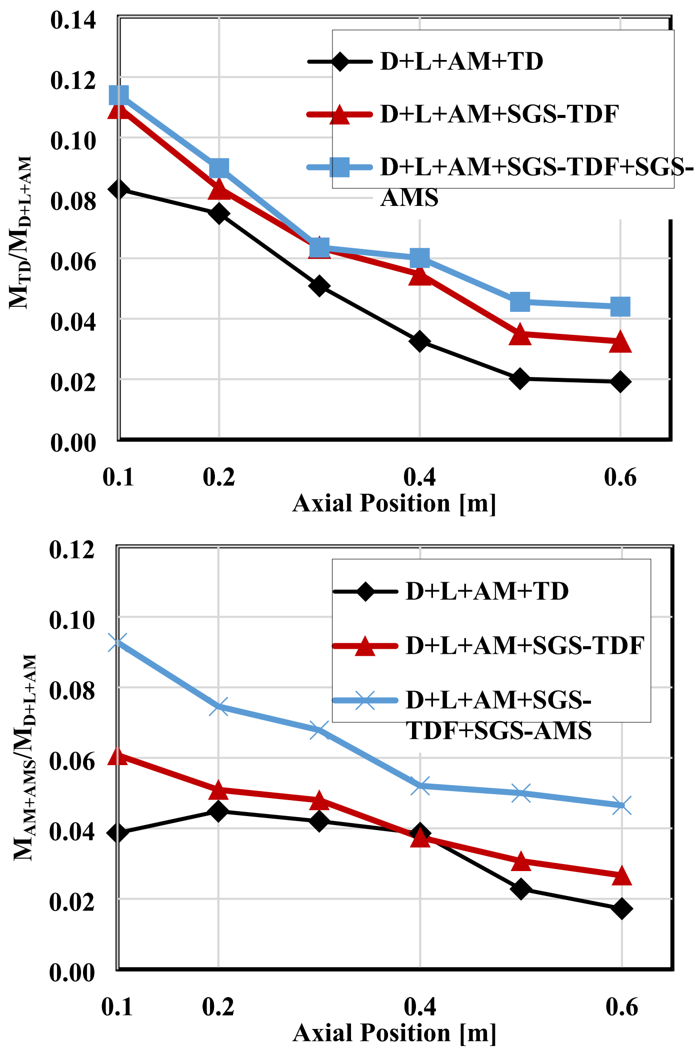

Figure 6

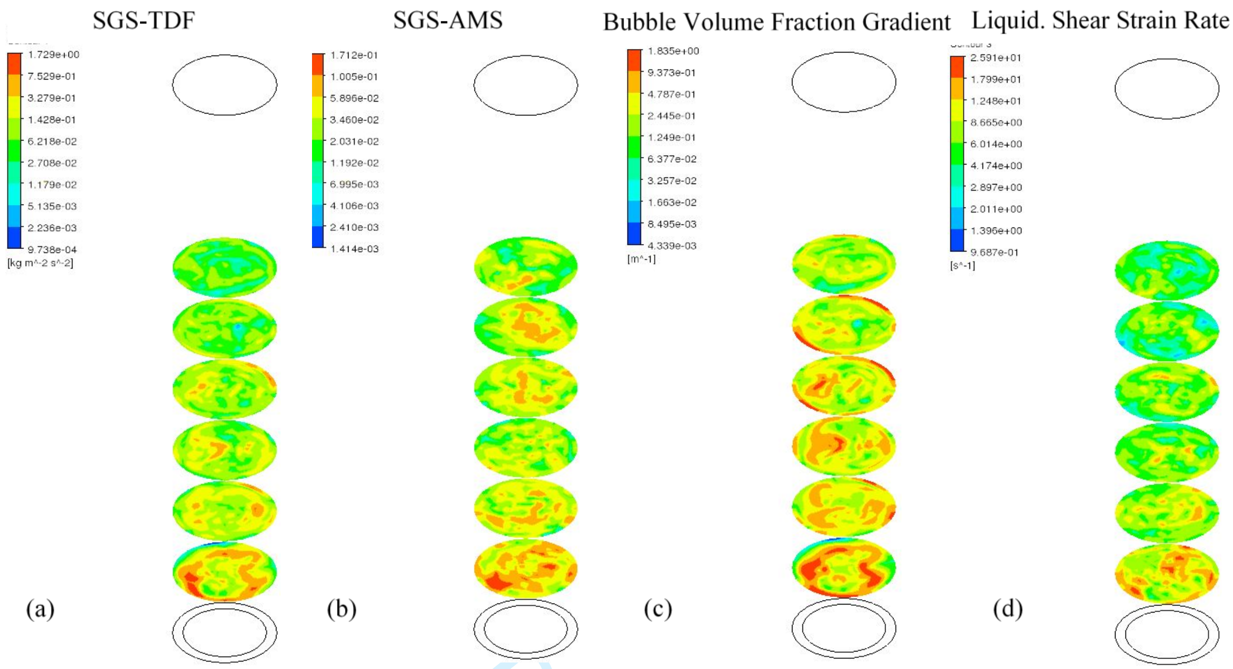

Figure 7

3.3 Effects of inclusion of turbulent dispersion and added mass stress on turbulent kinetic energy spectra and interfacial mass transfer

In order to assess the impact of inclusion of SGS-TDF and SGS-AMS models on the calculation of the turbulent kinetic energy of the liquid phase, the one-dimensional LES-filtered turbulent kinetic energy power spectral densities (PSD) $E_{11}(\kappa)$ obtained for Cases 1, 2 and 3 are presented in Figure 8. The liquid axial turbulent velocity is monitored at the centre of the cross section at z = 0.325 m. The turbulent energy spectrum is obtained by taking the Fast Fourier Transform (FFT) of the time correlation of axial turbulent velocity fluctuations based on the Welch method. As can be seen from Figure 8, the PSD predicted by using the modified SGS-TDF and SGS-AMS models can be still approximated and described by using Pope's model spectrum [16] but considering the bubble volume fraction influence and the relation between one-dimensional and three-dimensional spectrum, defined by

$$E_{11}(\kappa_{11}) = \int_{\kappa_{11}}^{\infty} \frac{E(\kappa)}{\kappa}\left(1-\frac{\kappa_1^2}{\kappa^2}\right)d\kappa$$

$$= \int_{\kappa_{11}}^{\infty} \frac{C(1-\alpha_G)\varepsilon^{2/3}\kappa^{-5/3}\left[\frac{\kappa L}{\sqrt{(\kappa L)^2+C_L}}\right]^{\frac{5}{3}+p_0} exp\left[-\beta\left\{\left[(\kappa\eta)^4+C_\eta^4\right]^{1/4}-C_\eta\right\}\right]}{\kappa}\left(1-\frac{\kappa_1^2}{\kappa^2}\right) d\kappa \quad (13)$$

The parameters β and p_0 are found to be equal to 5.2 and 2.0, respectively. The use of the modified SGS-TDF and SGS-AMS models gives a -5/3 scaling in smaller wave number zone while presents a -3 scaling law measured based on the wave number κ_1 larger than the typical wave number characterized by the equivalent bubble size, i.e. $\kappa_B = \frac{2\pi}{d_B} \approx 2464\ m^{-1}$. It can be seen from Figure 9(c) that the transition for different scaling laws in $E_{11}(\kappa)$ takes place in the wave number at about $\kappa_1 \approx 2500\ m^{-1}$, where the left of the transition location shows the -5/3 slope while the right side of the transition gives rise to the -3 scaling, clearly indicating the feature of feeding of bubble induced turbulence to the turbulent kinetic energy. This -3 scaling were also demonstrated by the experimental work as well as DNS [17-19].

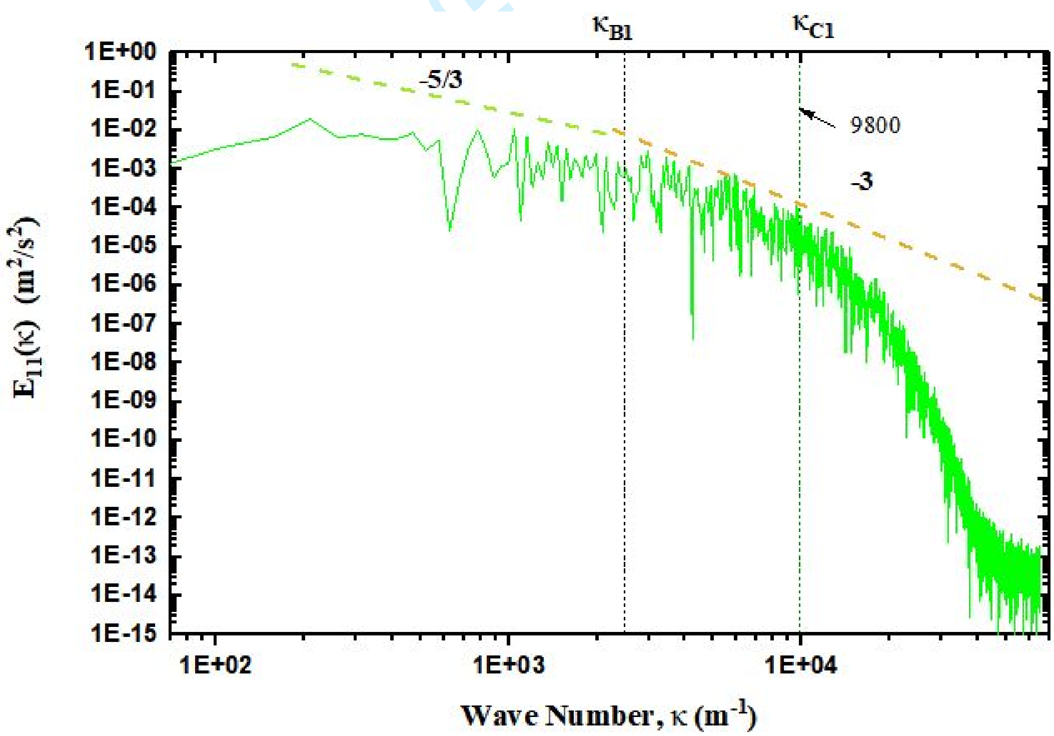

(a)

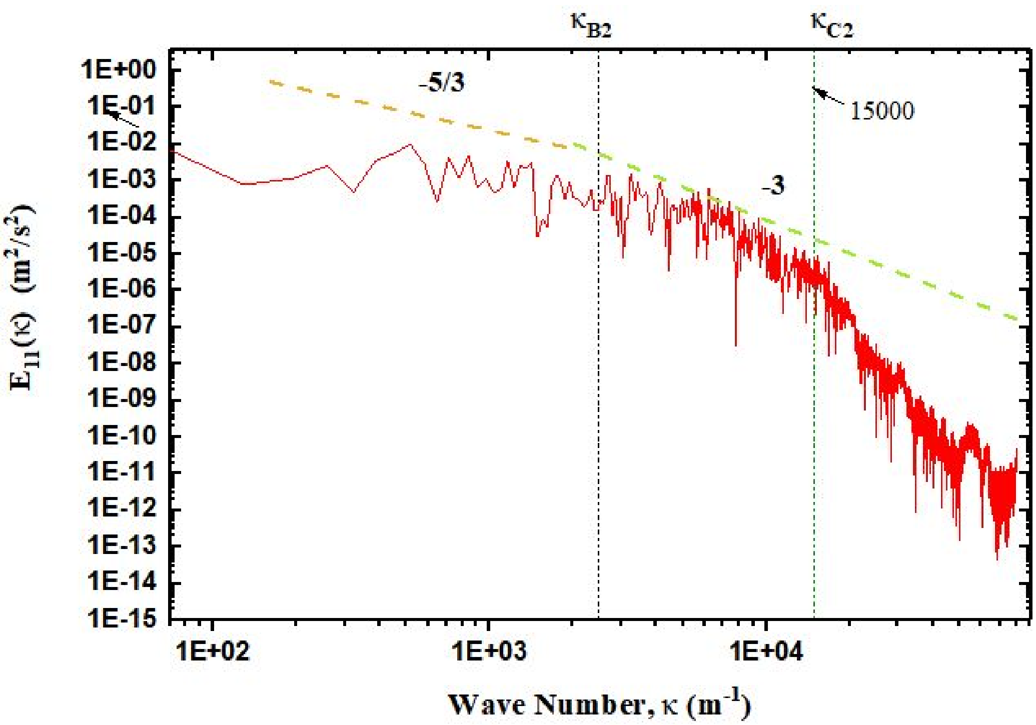
κB2
κC2
-5/3
15000
-3
E11(κ) (m2/s2)
1E+00
1E-01
1E-02
1E-03
1E-04
1E-05
1E-06
1E-07
1E-08
1E-09
1E-10
1E-11
1E-12
1E-13
1E-14
1E-15
1E+02
1E+03
1E+04
Wave Number, κ (m-1)

(b)

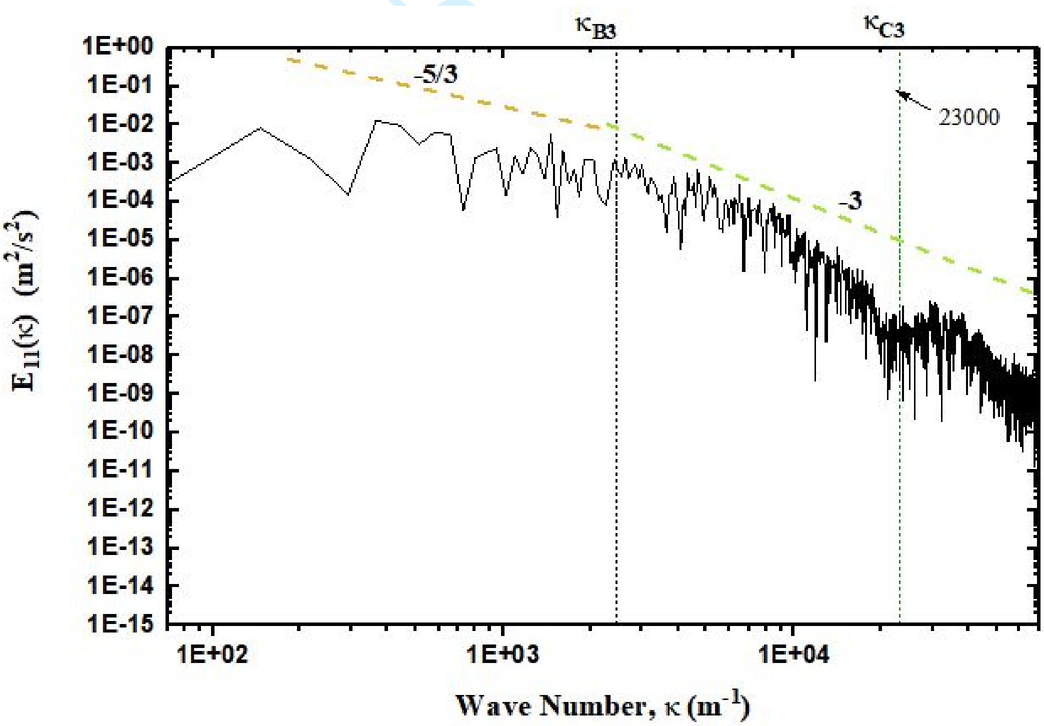
κB3
κC3
-5/3
23000
-3
E11(κ) (m2/s2)
1E+00
1E-01
1E-02
1E-03
1E-04
1E-05
1E-06
1E-07
1E-08
1E-09
1E-10
1E-11
1E-12
1E-13
1E-14
1E-15
1E+02
1E+03
1E+04
Wave Number, κ (m-1)

(c)

Figure 8

3.4 Spatial correlation between local bubble volume fraction and shear strain rate

In order to assess the effect of accounting the SGS-AMS on the evolution of bubble transport in the bubble column, the correlation between the local bubble volume fraction fluctuation and the added mass stress was assessed. The spatial correlation between the local bubble volume fraction and shear strain rate fluctuation to characterise the interaction of bubbles with SGS turbulent eddies along the axial height of the bubble column is proposed, defined by

$$R_{\alpha_G \bar{S}_{ij}}(\Delta h) = \frac{\overline{\alpha'_G(h_0)\left|\bar{S}'_{ij}(h_0+\Delta h)\right|}}{\sqrt{\alpha'^2_G(h_0)}\sqrt{\left|\bar{S}'^2_{ij}(h_0)\right|}} \quad (14)$$

Figure 9 presents the $R_{\alpha_G \bar{S}_{ij}}(\Delta h)$ variations along the centreline at different axial height from Δh = 0 to Δh = 0.325m of the bubble column. It can be seen from the figure that along the centreline, higher value of bubble volume fraction is always accompanied by larger variations in the correlation coefficient $R_{\alpha_G \bar{S}_{ij}}(\Delta h)$ along the height. The change of the turbulence induced shear strain rate strongly affect the entrainment of the bubbles, causing the local bubble volume fraction fluctuations as can be seen from Figure 10.

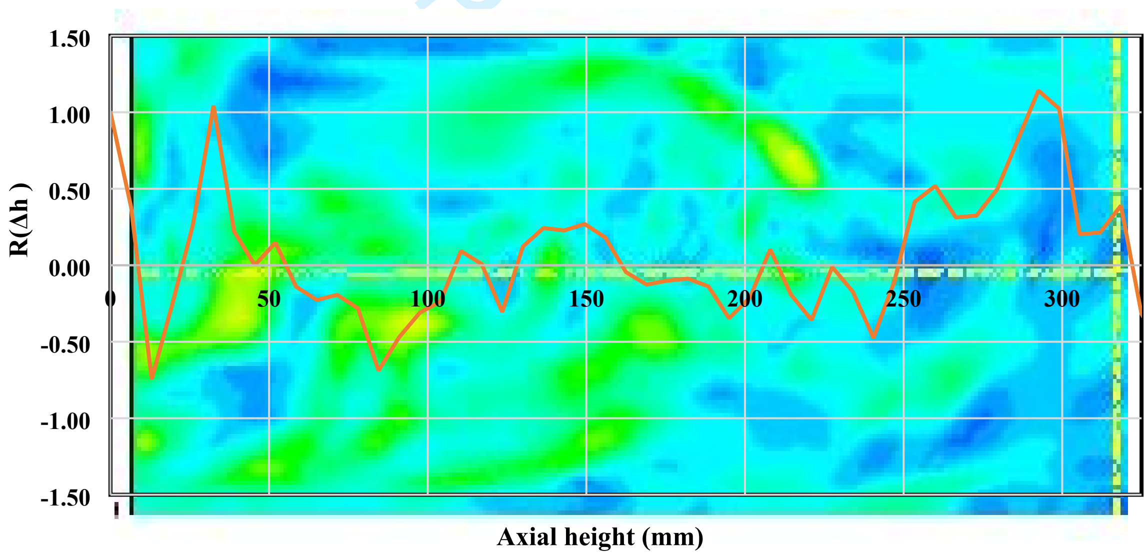

Figure 9

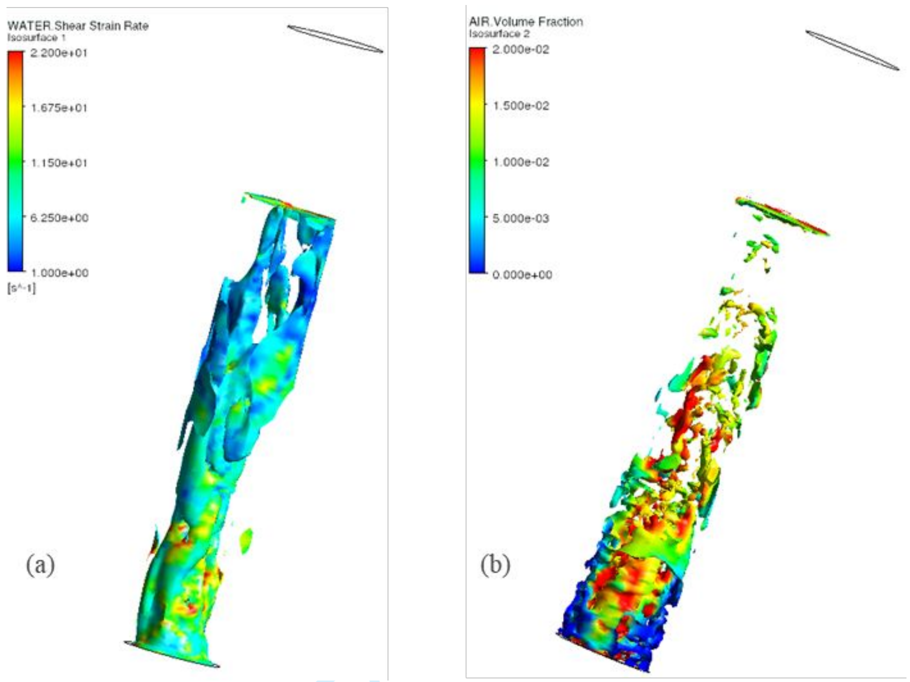

Figure 10

4. Conclusions

It was affirmed that bubble dynamics in the bubble column can be captured by using the adequate SGS-TDF and SGS-AMS models in Eulerian-Eulerian LES modelling, when mimicking the bubble transport in the bubble column. This can imply that the modified SGS-TDF and SGS-AMS models may play an equivalent role in indicating the bubble fluctuating motion predicted by using Euler/Lagrange LES modelling approach but with the stochastic dispersion model [4]. Though the case presented in the present study has been confined to a circular cylindrical bubble column, it has been revealed that the proposed modelling can be also applied to other cases such as square bubble column. The cross-sectional averaged absolute ratios of SGS-TDF force to the time averaged drag force and SGS-AMS force to the time averaged added mass force along the height of the bubble column are found to be around 5%-10% with the higher percentage taking place in the lower part of the column, indicating the needs to include the contributions from the SGS-TDF and SGS-AMS forces for radial re-distributing bubble volume fraction profiles. The SGS-TDF has more influences in the radial direction while the SGS-AMS has more influences in the main flow direction. The turbulent kinetic energy spectrum obtained at the given locations by jointly applying the modified SGS-TDF and SGS-AMS models has shown the existence of a -5/3 scaling law followed by an approximate -3 scaling law in the slope of the spectrum. In addition, a correlation of the local extra eddy viscosity and turbulent shear stresses gradients in both phases has been proposed.

Acknowledgements

This work was financially supported by the National Natural Science Foundation of China (Grant Nos. 21761132026, 91534118).

Symbols used

A	$[m^{-1}]$	Area density
C_D	[-]	Drag coefficient
C_{TD}	[-]	Turbulent dispersion coefficient
C_L	[-]	Lift coefficient
C_{AM}	[-]	Added mass coefficient
d	[m]	Bubble diameter
E_0	[-]	Eötvös number
f	[Hz]	Frequency
$\mathbf{M}_D$	$[N/m^3]$	Drag force
$\mathbf{M}_L$	$[N/m^3]$	Lift force
$\mathbf{M}_{AM}$	$[N/m^3]$	Added mass force
$\mathbf{M}_{AMS}$	$[N/m^3]$	Added mass stress force
$\mathbf{M}_{TD}$	$[N/m^3]$	Turbulent dispersion force
$\mathbf{g}$	$[m/s^2]$	Gravity acceleration
Q	$[s^{-2}]$	Invariant Q-criterion
Re	[-]	Reynolds number
S	$[s^{-1}]$	Characteristic filtered rate of strain
Sh	[-]	Sherwood number
Sc	[-]	Schmidt number
$\mathbf{u}$	[m/s]	Velocity vector
t	[s]	Time
ω	$[s^{-1}]$	Water vorticity

Greek letters

α	[-]	Phase volume fraction, gas holdup

σ_{TD}	[-]	Turbulent Schmidt number of gas phase
γ	[-]	Volume increment ratio
ν_t	$[m^2/s]$	Turbulent kinematic viscosity
ε	$[m^2/s^3]$	Turbulence dissipation rate
λ	[m]	Characteristic length scale of eddy
τ	[Pa]	Shear stress
μ	$[Pa \cdot s]$	Liquid dynamic viscosity
μ_{eff}	$[Pa \cdot s]$	Effective viscosity of the liquid phase
Δ	[m]	LES delta
κ	$[m^{-1}]$	Wave number
γ	[-]	Volume increment ratio

Subscripts

B	Bubble
G	Gas phase
L	Liquid phase
max	Maximum
SGS	Sub-grid scale
i	i-th component
j	j-th component

References

[1] H. Ayed, J. Chahed, V. Roig, *AIChE Journal*, **2007**, 53 (11), 2742-2753. DOI: 10.1115/icone18-29517.

[2] M.A. Atiya, A.M. Rahman, A. Abd Al-Jabbar, *Al-Khwarizmi Engineering Journal*, **2011**, 7 (4): 61-75.

[3] M. Rezig, G. Bellakhal, J. Chahed*, AIChE Journal*, **2017**, 63(9), 4214-4223. DOI: 10.1002/aic.15736.

[4] M. Sommerfeld, M. Muniz, T. Reichardt, *Journal of Chemical Engineering of Japan*, **2018**, 51(4), 301–317.

[5] N.G. Deen, T. Solberg, B.H. Hjertager, *Chemical Engineering Science*, **2001**, 56(21-22), 6341–6349.

[6] M. Sommerfeld, D. Broder, *Industrial & Engineering Chemistry Research*, **2009**, 48(1), 330–340.

[7] V.V. Buwa, V.V. Ranade, *Chemical Engineering Science*, **2002**, 57(22-23), 4715–4736.

[8] R. Rzehak, M. Krauß, P. Kováts, K. Zähringer, *International Journal of Multiphase Flow*, **2017**, 89, 299–312. DOI: 10.1016/j.ijmultiphaseflow.2016.09.024

[9] A. Kulkarni, K. Ekambara, J. Joshi, *Chemical Engineering Science*, **2007,** 62(4), 1049–1072.

[10] S. Long, J. Yang, X. Huang, G. Li, W. Shi, M. Sommerfeld, X. Yang, *International Journal of Heat and Mass Transfer*, **2020**, 161, 120240. DOI: 10.1016/j.ijheatmasstransfer.2020.120240

[11] D.A. Drew, S.L. Passman, *Theory of multicomponent fluids*, Springer Science & Business Media, **2006**.

[12] M. Bhole, J. Joshi, D. Ramkrishna, *Chemical Engineering Science*, **2008**, 63(8), 2267–2282. DOI: 10.1016/j.ces.2008.01.013

[13] Z. Huang, D.D. McClure, G.W. Barton, D.F. Fletcher, J.M. Kavanagh*, Chemical Engineering Science*, **2018,** 186, 88–101. DOI: 10.1016/j.ces.2018.04.025

[14] M. Milelli, *A numerical analysis of confined turbulent bubble plumes*, Ph.D. Thesis, ETH Zurich, **2002**.

[15] M. Muniz, M. Sommerfeld, *International Journal of Multiphase Flow*, **2020**, 128, 103256. DOI: 10.1016/j.ijmultiphaseflow.2020.103256

[16] S.B. Pope, *Turbulent flows*, IOP Publishing, **2001**.

[17] V.N. Prakash, J.M. Mercado, L. van Wijngaarden, E. Mancilla, Y. Tagawa, D. Lohse, C. Sun, *Journal of Fluid Mechanics*, **2016**, 791, 174–190. DOI: 10.1017/jfm.2016.49

[18] J.M. Mercado, D.C. Gomez, D. Van Gils, C. Sun, D. Lohse, *Journal of Fluid Mechanics*, **2010**, 650, 287–306. DOI: 10.1017/s0022112009993570

[19] G. Riboux, D. Legendre, F. Risso, *Journal of Fluid Mechanics*, **2013,** 719, 362–387. DOI: 10.1017/jfm.2013.12.

Figure 1. Schematic of contribution from SGS-TDF and SGS-AMS in bubbly flow.

Figure 2. Schematic of a bubble column with imaging system and data acquisition.

Figure 3. Schematic of mesh set-up in the bubble column for LES modelling.

Figure 4. Comparison of time-averaged bubble axial velocity distribution at z=325mm by using three models with experimental and numerical data obtained from Sommerfeld et al. (Dot: experimental data[4]; Dash: E-L simulation data [4].

Figure 5. Comparison of time-averaged normalized bubble volume fraction distribution at z=325mm by using three models with experimental and numerical data obtained from Sommerfeld et al. [15]

Figure 6. Quantification of (a) SGS turbulent dispersion force (TDF) contribution: and (b) total added mass force (AM) contribution: cross-sectional averaged AM over the sum of drag, lift and added mass force ratio along the bubble column height H=0.1-0.6m.

Figure 7. Distribution of (a) SGS-TDF; (b) SGS-AMS; (c) bubble volume fraction gradient; (d) liquid phase shear strain rate at different height from H=0.1-0.6m at t=100s in Case 3.

Figure 8. Predicted turbulent kinetic energy spectrum of liquid axial velocity at middle point at z=325mm by using (a) case 1: D+L+AM+TD; (b) case 2: D+L+AM+SGS-TDF; (c) case 2: D+L+AM+SGS-TDF+SGS-AMS.

Figure 9. Spatial correlation coefficient R_(α_G S̅_ij) (Δh) along the height of the bubble column from z=0 to z=325mm. The background was superimposed with the contours of instantaneous liquid phase shear strain rate at X=0, YZ-Plane.

Figure 10. Iso-surfaces of (a) bubble volume fraction $\alpha_B = 0.016$ colored by local water shear strain rate and (b) water shear strain rate $S_{ij,L} = 10\ s^{-1}$, colored by local bubble volume fraction at t =100s.

Table 1. Interphase force closure.

CEAT Graphic Abstract